actuators

MDPI

Article

Time-Optimal Current Control of Synchronous Motor Drives

Václav Šmídl *, Antonín Glac and Zdeněk Peroutka

Research and Innovation Centre for Electrical Engineering (RICE), University of West Bohemia, 30100 Plzeň, Czech Republic

* Correspondence: vsmidl@fel.zcu.cz

Abstract: We are concerned with the problem of fast and accurate tracking of currents in the general synchronous drive. The problem becomes complicated with decreasing available voltage, which is common in high-speed and field weakening regimes. The existing time-optimal controllers rely on a simplified model, ignoring stator resistance and differences in inductances. We derive a solution for the general model considering all parameters and show how the parameters affect the current trajectory. One simplifying assumption had to be made, but we show in simulation that it has a negligible impact on accuracy. The simplification allowed for the design of a feed-forward controller that has a low computational cost and can be easily implemented in realtime. We provide experimental validation of the controller on the developed IPMSM drive prototype of the rated power of 4.5 kW using conventional industrial DSP. The controller is compared to conventional PI and deadbeat solutions, demonstrating that the time-optimal controller can reach the required setpoint four times faster than the competitors at the field weakening regime of the drive. The proposed feed-forward control can be seen as a universal building block that can be combined with existing feedback controllers and observers and thus incorporated into existing control solutions.

Keywords: interior permanent magnet synchronous motor (IPMSM); maximum torque per ampere (MTPA); maximum torque per current (MTPC); dead beat control, predictive control

check for updates

Citation: Šmídl, V.; Glac, A.; Peroutka, Z. Time-Optimal Current Control of Synchronous Motor Drives. *Actuators* **2023**, *12*, 15. https://doi.org/10.3390/act12010015

Academic Editor: Shuxiang Dong

Received: 30 November 2022
Revised: 16 December 2022
Accepted: 21 December 2022
Published: 29 December 2022

Copyright: © 2022 by the authors. Licensee MDPI, Basel, Switzerland. This article is an open access article distributed under the terms and conditions of the Creative Commons Attribution (CC BY) license (https://creativecommons.org/licenses/by/4.0/).

1. Introduction

Control of synchronous motor drives is traditionally decomposed into nested loops where the current loop is the fastest of them. A prominent example is the conventional field-oriented control of using a cascade of PID controllers [1]. Since the time constants of the current loops are relatively short, the optimal operating points of the drive are usually given as inputs to the current control loop [2]. The optimal current setpoints are computed for steady-state operations, using well-known results such as the maximum torque per ampere MTPA curve [3]. Even in the calculation of the MTPA, the stator resistance of the drive is often neglected to achieve simpler solutions. This restriction has been recently relaxed by designing optimal steady-state references for the full electric model of a synchronous motor drive [4].

Optimization of the steady state operation is typically considered for permanent operation of the drive, with application to pumps or ventilation, hence the most common concern of optimization is efficiency [4,5]. However, this optimization is incomplete for highly dynamic operations such as robotic actuators or manipulators, where high precision of set-point tracking is required. In such applications, the set-point trajectory is often known in advance, allowing optimization of the feed-forward part of the controller. In this paper, we focus on feed-forward optimization of the current loop. All other aspects of the control, such as set-point design [4], feed-back part of the control [6], and disturbance rejection [7,8] will be briefly commented at the end of the paper.

Computation of the optimal feed-forward trajectories for transients can be achieved numerically, using model predictive control [9]. However, even many predictive control solutions often use steady-state solutions [10,11] or decomposition into speed and current

loop [12,13]. While MPC can also be utilized on a higher level with beneficial results [14,15], its application to demanding current control transients is not successful. The reason is the hard constraint on the input voltage. Due to this constraint, a very long prediction horizon is required to obtain the optimal current trajectory with a completely different trajectory for shorter horizons [16]. The results of long-horizon optimization are counter-intuitive, since the optimal current profile is increasing the tracking error at the beginning of the transient. The reason is that it will reach the set-point in a shorter time than if it tried to decrease the error. This solution can be obtained numerically with very high computational cost. While it is possible to transform the numerical solution to explicit model predictive control [12,17], any change in motor parameters requires recomputing of the expensive solution.

In this paper, we address this problem using time-optimal control (TOC) methods [18]. Minimizing the time to convergence can be treated using general-purpose methods [19]; however, some problems allow for an analytical solution. Specifically, we will be formalizing the current control problem in continuous time, where it can be addressed using Pontryagin's principle of maxima. This technique has been applied to the current control of PMSM drive problem, which has been studied in [20,21] using highly simplifying assumptions, such as neglected resistance. The solution of the full model problem is conceptually known [22,23]; however, its evaluation for the full model is non-trivial. It can be found, e.g., by dynamic programming [24], which is computationally demanding. An extension considering resistance has been presented in [25]; however, without considering different inductances in the direct and quadrature axis. In essence, the TOC serves to generate current setpoints for low level controllers such as deadbeat [2,26].

The contributions of our paper are as follows:

1. We review existing time-optimal current control methods.
2. We derive the explicit formula for the general case of a synchronous motor drive model, including stator resistance and different d- and q-axis inductances.
3. We provide simplification of the exact formula that allows real-time evaluation of the solution without a significant increase in computational complexity in comparison to previous approaches.
4. We demonstrate the advantage of the new proposed general formula over the previous solutions in torque-controlled IPMSM drive in simulations with various parameters.
5. The solution was implemented in real-time digital signal processor and experimentally validated on a drive prototype of the rated power of 4.5 kW.

The paper is organized as follows. The review of previous approaches is summarized in Section 2. The general formula of time-optimal control is derived in Section 3. A sensitivity study of the proposed control to parameters of the drive is performed in Section 4 using simulation. The experimental comparison with a deadbeat controller and the PI controller is reported in Section 5.

2. Review of Existing Approaches

2.1. Mathematical Model of Synchronous Motor Drive

Mathematical model of a synchronous motor drive in the dq reference frame linked to a rotor flux linkage vector is generally described by stator flux dynamics [4]

$$\dot{\boldsymbol{\psi}}_s(t) = -R_s \boldsymbol{i}_s(t) - \omega(t) \boldsymbol{J} \boldsymbol{\psi}_s(t) + \boldsymbol{u}_s(t), \tag{1}$$

where $\boldsymbol{\psi}_s$ denotes the vector of stator flux in the dq reference frame, $\omega(t)$ is the electrical rotor speed, R_s is the stator winding resistance, $\boldsymbol{J}$ is the rotation matrix $\boldsymbol{J} = [0, -1; 1, 0]$ and $\boldsymbol{u}_s(t)$ is the stator voltage vector in the dq reference frame. We will assume that the flux can be (at least locally) approximated by linear formula

$$\boldsymbol{\psi}_s(t) = \boldsymbol{L}_s \boldsymbol{i}_s(t) + \boldsymbol{\psi}_{\mathrm{pm}}, \tag{2}$$

where we assume a diagonal matrix of inductances $\boldsymbol{L}_s = [L_{s,d}, 0; 0, L_{s,q}]$ and flux excited by the permanent magnets on the rotor $\boldsymbol{\psi}_{\text{pm}} = [\psi_{\text{pm},d}; \psi_{\text{pm},q}]$. In this work, we consider $\boldsymbol{\psi}_{\text{pm}}$ to be a general constant vector, which can be specialized for particular drives by setting its elements to zero [4]. For example, $\boldsymbol{\psi}_{\text{pm},q} = 0$ for PMSM and PM-enhanced RSM, $\psi_{\text{pm},d} = 0$ for PM-assisted RSM, and $\boldsymbol{\psi}_{\text{pm}} = [0; 0]$ for RSM drive. We will derive all equations for the general synchronous motor model.

Since we are concerned with drives that have a much faster current response than mechanical dynamics, we will consider the rotor speed ω to be constant during the transient. The state variable is thus the vector of fluxes $\boldsymbol{x} = \boldsymbol{\psi} = [\psi_{s,d}; \psi_{s,q}]$, with the control variable $\boldsymbol{u} = \boldsymbol{u}_s$ and with dynamics

$$\dot{\boldsymbol{x}}(t) = \boldsymbol{A}\boldsymbol{x}(t) + \boldsymbol{u}(t) + \boldsymbol{q}, \tag{3}$$

where

$$\boldsymbol{A} = -R_s \boldsymbol{L}_s^{-1} - \omega \boldsymbol{J}, \qquad \boldsymbol{q} = R_s \boldsymbol{L}_s^{-1} \boldsymbol{\psi}_{\text{pm}}.$$

The trajectory of the system is thus

$$\boldsymbol{x}(t) = e^{t\boldsymbol{A}} \left(\boldsymbol{x}(0) + \int_0^t e^{-s\boldsymbol{A}} (\boldsymbol{u}(s) + \boldsymbol{q}) ds \right). \tag{4}$$

2.2. Time-Optimal Control (TOC)

Time-optimal control is a special case of optimal control where the aim is to reach the desired state $\boldsymbol{x}_{\text{des}}$ from the original state $\boldsymbol{x}_0$ in the minimum possible time τ. The well-known Pontryagin principle of maxima [18] states necessary conditions for the optimal trajectory $\boldsymbol{x}^*$ and optimal control $\boldsymbol{u}^*$ via two dynamic equations

$$\dot{\boldsymbol{x}}^*(t) = \frac{\partial H}{\partial \boldsymbol{p}}(t) = \boldsymbol{A}\boldsymbol{x}^*(t) + \boldsymbol{u}^*(t) + \boldsymbol{q}(t),$$
$$\dot{\boldsymbol{p}}(t) = -\frac{\partial H}{\partial \boldsymbol{x}}(t) = -\boldsymbol{A}^T \boldsymbol{p}(t),$$

and two boundary conditions $\boldsymbol{x}(0) = \boldsymbol{x}_0$ and $\boldsymbol{x}(\tau) = \boldsymbol{x}_{\text{des}}$. Here, $H(\boldsymbol{p}(t), \boldsymbol{x}(t), \boldsymbol{u}(t)) = 1 + \boldsymbol{p}(t)^T (\boldsymbol{A}\boldsymbol{x}(t) + \boldsymbol{u}(t) + \boldsymbol{q})$ is the Hamiltonian of the system, and $\boldsymbol{p}$ is known as the costate (adjoint) variable satisfying

$$\boldsymbol{p}(t) = e^{-t\boldsymbol{A}^T} \boldsymbol{p}_0. \tag{5}$$

The optimal control $\boldsymbol{u}(t)$ has to satisfy for almost every $t \in [0, \tau]$ the maximum principle

$$H(\boldsymbol{p}(t), \boldsymbol{x}^*(t), \boldsymbol{u}^*(t)) = \max(H(\boldsymbol{p}(t), \boldsymbol{x}^*(t), \boldsymbol{u}(t)))$$
$$s.t.\ ||\boldsymbol{u}(t)|| \leq \overline{U}. \tag{6}$$

Under the circular voltage constraint (6), the optimal control has the form

$$\boldsymbol{u}(t) = \overline{U} \frac{\boldsymbol{p}(t)}{||\boldsymbol{p}(t)||}. \tag{7}$$

Substituting (7) into (4), we obtain

$$\boldsymbol{x}(t) = e^{t\boldsymbol{A}} \left(\boldsymbol{x}_0 + \int_0^t \left[\overline{U} \frac{e^{-s\boldsymbol{A}} e^{-s\boldsymbol{A}^T} \boldsymbol{p}_0}{\sqrt{\boldsymbol{p}_0 e^{-s\boldsymbol{A}} e^{-s\boldsymbol{A}^T} \boldsymbol{p}_0}} + e^{-s\boldsymbol{A}} \boldsymbol{q} \right] ds \right). \tag{8}$$

Solving (8) together with constraint $\boldsymbol{x}(\tau) = \boldsymbol{x}_{\text{des}}$ for τ and $\boldsymbol{p}_0$ yields the required solution. Note that we may normalize the costate by setting $||\boldsymbol{p}_0|| = 1$. The complexity of the solution depends highly on the model matrix $\boldsymbol{A}$.

2.3. TOC with Neglected Stator Resistance

To our best knowledge, all previous approaches such as [20,21,24], were designed with neglected stator resistance $R_s \approx 0$. It is understandable because this assumption is very convenient and allows us to greatly simplify the problem, since $\boldsymbol{A} = -\omega \boldsymbol{J}$ and $\boldsymbol{q} = 0$. Then,

$$e^{t\boldsymbol{A}} = \begin{bmatrix} \cos\omega t & \sin\omega t \\ -\sin\omega t & \cos\omega t \end{bmatrix}, \quad e^{-s\boldsymbol{A}} e^{-s\boldsymbol{A}^T} = I,$$

Using assumption $||\boldsymbol{p}_0|| = 1$, Equation (8) becomes

$$\boldsymbol{x}(t) = e^{t\boldsymbol{A}}(\boldsymbol{x}_0 + \overline{U}\boldsymbol{p}_0 t). \tag{9}$$

Substituting $t = \tau$ and using the terminal condition $\boldsymbol{x}(\tau) = \boldsymbol{x}_{\text{des}}$ in (9) yields $\boldsymbol{p}_0 = \frac{1}{\overline{U}\tau}(e^{-\tau\boldsymbol{A}}\boldsymbol{x}_{\text{des}} - \boldsymbol{x}_0)$. Since $\boldsymbol{p}_0$ has to satisfy the normalization condition $||\boldsymbol{p}_0|| = 1$, we obtain an implicit equation:

$$||e^{-\tau\boldsymbol{A}}\boldsymbol{x}_{\text{des}} - \boldsymbol{x}_0||^2 = (\overline{U}\tau)^2, \tag{10}$$

where the only free variable is τ. Finding the solution of (10) can be done using, e.g., the bisection method.

3. Time-Optimal Flux Control Considering Stator Resistance

Since the assumption of negligible resistance is not valid in many cases, we now use the study solution of the time-optimal control (7) for more general cases. First, we will analyze the case of equal inductances $L_{s,d} \approx L_{s,q}$, which is a reasonable assumption for surface mounted PMSM. The more general case is studied subsequently.

3.1. TOC with Equal Stator Inductances

Under the assumption of equal stator inductances in the d and q axes, $L_s = L_{s,d} = L_{s,q}$ the system (3) has the form

$$\boldsymbol{A} = -\rho\boldsymbol{I} - \omega\boldsymbol{J}, \quad \boldsymbol{q} = \rho\boldsymbol{\psi}_{\text{pm}},$$

where $\rho = R_s/L_s$, yielding

$$e^{t\boldsymbol{A}} = e^{-\rho t}\begin{bmatrix} \cos\omega t & -\sin\omega t \\ \sin\omega t & \cos\omega t \end{bmatrix}, \quad e^{-s\boldsymbol{A}} e^{-s\boldsymbol{A}^T} = e^{2\rho t}\boldsymbol{I}, \tag{11}$$

then, Equation (8) becomes

$$\boldsymbol{x}(t) = e^{t\boldsymbol{A}}\left(\boldsymbol{x}_0 + \int_0^t \left[e^{\rho s}\overline{U}\boldsymbol{p}_0 + e^{-s\boldsymbol{A}}\boldsymbol{q}\right] ds\right) \tag{12}$$

$$= e^{t\boldsymbol{A}}\left(\boldsymbol{x}_0 + \boldsymbol{A}^{-1}(\boldsymbol{I} - e^{-t\boldsymbol{A}})\boldsymbol{q} + \frac{\overline{U}}{\rho}(e^{\rho t} - 1)\boldsymbol{p}_0\right). \tag{13}$$

This yields an explicit form for the initial condition

$$\boldsymbol{p}_0 = \frac{\rho}{\overline{U}(e^{\rho t} - 1)}\left(e^{-t\boldsymbol{A}}\boldsymbol{x}(t) - \boldsymbol{x}_0 - \boldsymbol{A}^{-1}(\boldsymbol{I} - e^{-t\boldsymbol{A}})\boldsymbol{q}\right) \tag{14}$$

which once again has to be normalized and together with $\boldsymbol{x}(\tau) = \boldsymbol{x}_{\text{des}}$ yield

$$||e^{-t\boldsymbol{A}}\boldsymbol{x}_{\text{des}} - \boldsymbol{x}_0 - \boldsymbol{A}^{-1}(\boldsymbol{I} - e^{-\boldsymbol{A}t})\boldsymbol{q}||^2 = \left(\frac{\overline{U}}{\rho}(e^{\rho t} - 1)\right)^2. \tag{15}$$

When multiplying this formula by $e^{-\rho\tau}$, the vector on the left-hand side can be simplified and the whole formula results in

$$0 = \left(\frac{\overline{U}}{\rho}(1-e^{-\rho\tau})\right)^2 - \left(-\alpha_1\cos\omega\tau + \alpha_2\sin\omega\tau + \beta_1 e^{-\rho\tau}\right)^2 - \left(-\alpha_2\cos\omega\tau - \alpha_1\sin\omega\tau + \beta_2 e^{-\rho\tau}\right)^2. \quad (16)$$

where

$$\alpha_1 = \psi_{\mathrm{des},d} - \frac{\rho\psi_{\mathrm{pm},d} + \omega\psi_{\mathrm{pm},q}}{\rho^2+\omega^2}\rho, \qquad \beta_1 = \psi_{0,d} - \frac{\omega\psi_{\mathrm{pm},q} + \rho\psi_{\mathrm{pm},d}}{\rho^2+\omega^2}\rho,$$
$$\alpha_2 = \psi_{\mathrm{des},q} + \frac{\omega\psi_{\mathrm{pm},d} - \rho\psi_{\mathrm{pm},q}}{\rho^2+\omega^2}\rho, \qquad \beta_2 = \psi_{0,q} + \frac{\omega\psi_{\mathrm{pm},d} - \rho\psi_{\mathrm{pm},q}}{\rho^2+\omega^2}\rho. \quad (17)$$

This is one equation in the time variable and thus of complexity comparable to that of (10). The only increase is due to the need to evaluate the exponential function. However, accurate approximations for its evaluation are available [27].

3.2. Different d, q Inductances

The assumption of the previous section is no longer valid in drives that have significantly different inductances. Since we use flux as the main variable, different inductances influence only the stator resistance dependent terms of Equation (3) via $R_s L_{s,d}^{-1}$ and $R_s L_{s,q}^{-1}$. For analytical convenience, we denote $\rho = \frac{1}{2}R_s(L_{s,d}^{-1} + L_{s,q}^{-1})$ and $\delta = \frac{1}{2}R_s(L_{s,d}^{-1} - L_{s,q}^{-1})$. Then, (3) has the form

$$\boldsymbol{A} = -\begin{bmatrix}\rho+\delta & 0\\ 0 & \rho-\delta\end{bmatrix} - \omega\boldsymbol{J}. \quad (18)$$

The form of the system trajectory via the matrix exponential (4) then depends on the relation between δ and ω. Specifically, if $\omega > \delta$, the trajectory is periodic in the base of sin and cos functions just like (11), but with a different frequency $\sqrt{\omega^2-\delta^2}$. When $\delta > \omega$, the trajectory becomes aperiodic with parameter $\sqrt{\delta^2-\omega^2}$. When $\omega = \delta$, the trajectory becomes a straight line. To achieve compact notation for all cases, we introduce auxiliary variables:

$$c_1 = \sqrt{|\omega^2-\delta^2|},$$
$$c_2 = \delta^2 - \omega^2 - \rho^2,$$

and auxiliary functions $\sigma(t)$ and $\mu(t)$, defined as:

$$\begin{cases}\sigma(t) = \dfrac{\sin(c_1 t)}{c_1} & \mu(t) = \cos(c_1 t) & \text{for } |\delta| < |\omega|,\\ \sigma(t) = \dfrac{\sinh(c_1 t)}{c_1} & \mu(t) = \cosh(c_1 t) & \text{for } |\delta| > |\omega|,\\ \sigma(t) = t & \mu(t) = 1 & \text{for } |\delta| = |\omega|.\end{cases} \quad (19)$$

Note that the last equation is a limit of both former cases for $c_1 \to 0$.
Using auxiliary functions (19), the system dynamics can be written as

$$e^{t\boldsymbol{A}} = e^{-\rho t}\begin{bmatrix}\mu(t)-\delta\sigma(t) & \omega\sigma(t)\\ -\omega\sigma(t) & \mu(t)+\delta\sigma(t)\end{bmatrix}. \quad (20)$$

In this case, the norm of the costate, $||\boldsymbol{p}_0||$, required in (7) is rather complex and analytical expression of (5) becomes intractable. Therefore, we will proceed with the same normalization as in the case of PMSM, which is now an approximation:

$$e^{-s\boldsymbol{A}}e^{-s\boldsymbol{A}^T} \approx e^{2\rho t}, \tag{21}$$

validity of this approximation will be tested in simulation.

Under this approximation, the solution of the costate equation becomes formally equal to (14), giving an implicit equation very similar to (16):

$$0 = \left(\frac{\overline{U}}{\rho}(1-e^{-\rho\tau})c_2\right)^2 - \left(\alpha_1\mu(\tau)+\alpha_2\sigma(\tau)+\beta_1 e^{-\rho\tau}\right)^2 - \left(\alpha_3\mu(\tau)+\alpha_4\sigma(\tau)+\beta_2 e^{-\rho\tau}\right)^2. \tag{22}$$

where the only difference is in different constants

$$\begin{aligned}
\alpha_1 &= c_2\psi_{\mathrm{des},d} - \delta q_1 + \omega q_2 + q_1\rho,\\
\alpha_2 &= q_1\omega^2 - q_1\delta^2 + \delta c_2\psi_{\mathrm{des},d} + \delta q_1\rho - \omega c_2\psi_{\mathrm{des},q} - \omega q_2\rho,\\
\alpha_3 &= c_2\psi_{\mathrm{des},q} + \delta q_2 - \omega q_1 + q_2\rho,\\
\alpha_4 &= q_2\omega^2 - q_2\delta^2 - \delta c_2\psi_{\mathrm{des},q} - \delta q_2\rho + \omega c_2\psi_{\mathrm{des},d} + \omega q_1\rho,\\
\beta_1 &= -\omega q_2 - c_2\psi_{0,\mathrm{d}} + \delta q_1 - q_1\rho,\\
\beta_2 &= -\delta q_2 - c_2\psi_{0,\mathrm{q}} + \omega q_1 - q_2\rho.
\end{aligned} \tag{23}$$

Note that since these constants are independent of the time, they can be computed only once before the bisection method.

When the time of the transient τ is known, it is substituted to (14) to obtain $\boldsymbol{p}_0$, which is then substituted to (7) to obtain $\boldsymbol{u}^*(0)$:

$$u_d^* = \frac{\rho}{(1-e^{-\rho\tau})c_2}\left(\alpha_1\mu(\tau)+\alpha_2\sigma(\tau)+\beta_1 e^{-\rho\tau}\right), \tag{24}$$

$$u_q^* = \frac{\rho}{(1-e^{-\rho\tau})c_2}\left(\alpha_3\mu(\tau)+\alpha_4\sigma(\tau)+\beta_2 e^{-\rho\tau}\right). \tag{25}$$

3.3. Implementation Details

3.3.1. Time Discretization

The proposed controller is designed in continuous time; however, its implementation will be done in discrete time. Let us denote the time instant at which we will apply the controller by time index u_t. The time required to compute the solution prevents the use of the measurement at the same time. Hence, we assume that we have only one-step delayed measurement, $\boldsymbol{i}_{t-1}$. Therefore, we have to perform delay compensation, i.e., the initial state $\boldsymbol{x}_0$ is calculated using one-step ahead prediction (2). This value and the requested state $\boldsymbol{x}_{\mathrm{req}}$ are substituted into the implicit Equation (16). The solution of this equation using the bisection method is a scalar value τ^*, which is substituted into (24) and (25), which is the time-optimal control law.

3.3.2. Multiple Extremes in Bisection

To use the bisection method, we need to define the minimum and maximum of the search interval such that the function in these points have opposite signs. A suitable choice of the lower bound is zero, where the implicit function (22) is always positive. The upper bound is more problematic. One possible choice is setting the upper limit to the maximum expected time of a transient (e.g., 512 sampling periods, Δt). This setting becomes problematic at a very high speed regime in the field weakening operation. At this region, the current trajectory starts circulating and may cross the requested value multiple

times in a short window. The implicit function then has multiple roots, see Figure 1, and we need to select the one closest to zero. An optimal solution would be to derive an analytic upper bound on it. However, in the experimental evaluation, we use a simple heuristic solution. Specifically, we choose $t_{max} = 256\Delta t$, but the first evaluation is not made in the middle of the interval but at point $10\Delta t$. All subsequent evaluations are done using the standard bisection algorithm. We found that 20 steps of the bisection algorithm for solving Equation (22) are sufficient.

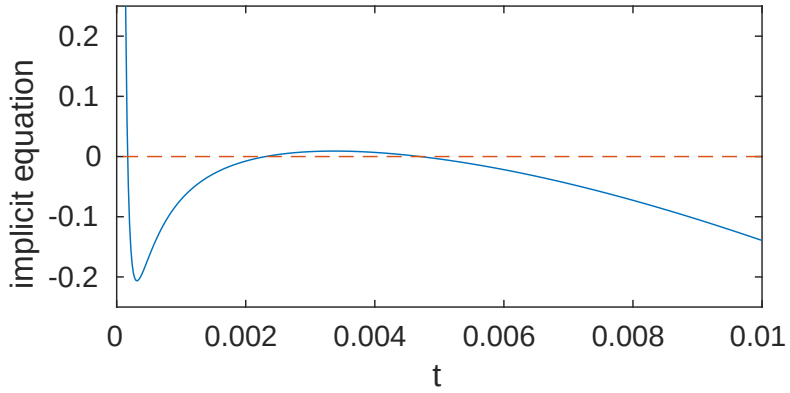

Figure 1. An example of multiple roots in the implicit Equation (22).

3.3.3. Small Step Solution

Another problem arises when the trajectory becomes too close to the requested value and $\tau < \Delta t$. In such a case, we compute the reference value for the PWM using the conventional deadbeat solution, which arises from the discrete-time version of model (3)

$$\frac{\boldsymbol{x}_{t+1} - \boldsymbol{x}_t}{\Delta t} = \boldsymbol{A}\boldsymbol{x}_t + \boldsymbol{u}_t + \boldsymbol{q},$$

where it is assumed that the requested value $\boldsymbol{x}^*$ can be reached in one step, yielding

$$\boldsymbol{u}_t^{\mathrm{DB}} = \frac{\boldsymbol{x}^* - \boldsymbol{x}_t}{\Delta t} - \boldsymbol{A}\boldsymbol{x}_t - \boldsymbol{q}. \tag{26}$$

When the state $\boldsymbol{x}_t$ is close to the requested value, the deadbeat solution is within the voltage limit. However, it becomes suboptimal when the amplitude of the solution $|\boldsymbol{u}_t^{\mathrm{DB}}|$ is higher than $\overline{U}$. This motivates the proposed algorithm for evaluation of the current control $\boldsymbol{u}_t^{\mathrm{opt}}$, Algorithm 1.

Algorithm 1 Time-optimal current control algorithm.

Input: measured current vector $\boldsymbol{i}_{t-1}$, requested current $\boldsymbol{i}_{\mathrm{des}}$

1. transform measured current to flux $\boldsymbol{x}_{t-1} = \boldsymbol{\psi}_{t-1}$, and $\boldsymbol{x}_{\mathrm{des}} = \boldsymbol{\psi}_{\mathrm{des}}$ using (2),
2. evaluate delay compensation $\boldsymbol{x}_t$ using Euler approximation of (3),
3. compute the deadbeat solution $\boldsymbol{u}_t^{\mathrm{DB}}$ using (26),
4. **if** $|\boldsymbol{u}_t^{\mathrm{DB}}| < \overline{U}$,
   assign $\boldsymbol{u}_t^{\mathrm{opt}} = \boldsymbol{u}_t^{\mathrm{DB}}$
   else
   find τ bisecting (16),
   evaluate $\boldsymbol{u}_t^{\mathrm{opt}}$ using (24) and (25),
5. compute modulation signal from $\boldsymbol{u}_t^{\mathrm{opt}}$.

The deadbeat solution alone is often used for current control [2]. However, in such a case, it has to be truncated to the voltage limit. Typical solution is

$$\boldsymbol{u}_t^{\mathrm{DBt}} = \begin{cases} \boldsymbol{u}_t^{\mathrm{DB}} & \text{if } |\boldsymbol{u}_t^{\mathrm{DB}}| < \overline{U}, \\ \frac{\overline{U}}{|\boldsymbol{u}_t^{\mathrm{DB}}|}\boldsymbol{u}_t^{\mathrm{DB}} & \text{otherwise.} \end{cases} \tag{27}$$

which we will use for comparison with the proposed TOC. The key difference between DB and TOC is the situation when the available voltage cannot satisfy the requirement in one step (i.e., the "else" part of step 4 in Algorithm 1).

Note that both algorithms are feed-forward controllers, relying on model correctness. Potentially this may lead to a small steady-state error, which can be compensated by an additional feedback controller. However, we have not experienced any steady state error in our experiments.

4. Simulations

In this section, we study the difference between the proposed solution and previous solutions that neglect stator resistances and different inductances on the time-optimal trajectory. First, we use the parameters of our experimental rig and then we study the sensitivity of the solution to parameter variations. All simulations were done in Matlab, without the use of any toolbox, since the simulation is fully determined by elementary arithmetic operations.

4.1. Nominal Parameters

Our experimental rig has the parameters

$$\begin{aligned} R_s &= 1.8\ \Omega, & \psi_{pm,d} &= 0.438\ \mathrm{Wb}, \\ L_{s,d} &= 14.0\ \mathrm{mH}, & \Delta t &= 100\ \mu\mathrm{s}, \\ L_{s,q} &= 19.3\ \mathrm{mH}, & U_{dc} &= 450\ \mathrm{V}. \end{aligned} \tag{28}$$

We compare three different methods for time-optimal flux control: (i) control with neglected resistance [20,23], (ii) solution with equal inductances, where the inductance is set to mean value of the true machine parameters, $L_s = 0.5(L_{s,d} + L_{s,q})$, and (iii) the proposed method with full model parameters. The methods are compared on a step change of the requested stator current from zero to $i_d^* = -3\mathrm{A}, i_q^* = 14\mathrm{A}$. The current trajectories of different control strategies are displayed in Figure 2.

In two modes, open-loop (left) and closed-loop (right). The open loop trajectory applies the control strategy designed at the origin. In the closed loop, the strategy is recomputed at every sampling period. For comparison, the deadbeat control (27) is also computed and displayed in the right column of Figure 2. Note that all time-optimal control strategies are relatively close to each other. This indicates that the effect of resistance on the trajectory is low. In contrast, the deadbeat controller (27) takes a different path. The difference is in the time to reach the setpoints. While for $\omega = 10$ rad/s all controllers reach the setpoint in 16 sampling periods, for $\omega = 400$ rad/s, all time-optimal controllers reach the setpoint in 46 sampling periods ($46\Delta t$), but the deadbeat reaches the setpoint in $131\Delta t$.

4.2. Sensitivity Study

The difference between all versions of the time-optimal control becomes more obvious when the ratio ρ between the resistance and inductance is higher. This is simulated by setting smaller values of the inductances, with $L_{s,d} > L_{s,q}$, namely $L_{s,d} = 5\,\mathrm{mH}$, $L_{s,q} = 3\,\mathrm{mH}$. The resulting current trajectories for all tested algorithms and step change of the requested stator current from zero to $[5, 30]\mathrm{A}$ are displayed in Figure 3.

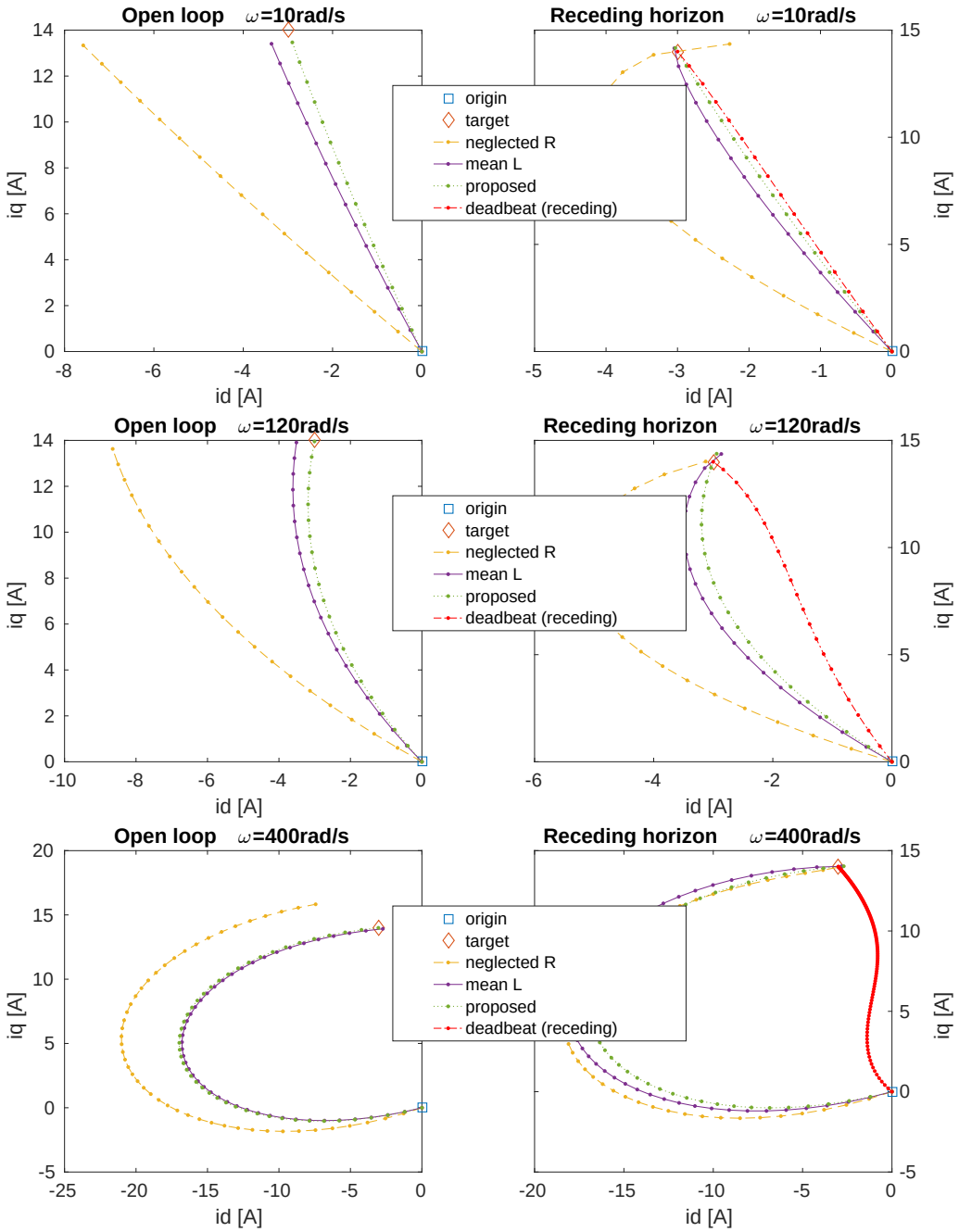

Figure 2. Comparison of studied versions of time-optimal control and deadbeat control on stator current reference step change from zero to $[-3, 14]$A for $\omega = 10$ rad/s (**top** row), $\omega = 120$ rad/s (**middle** row), and $\omega = 400$ rad/s (**bottom** row). The difference of the solutions in the origin is visible in the open-loop strategy (**left**), its impact on the receding horizon reevaluation in each sampling period (**right**), sampling times are denoted by dots on the full lines.

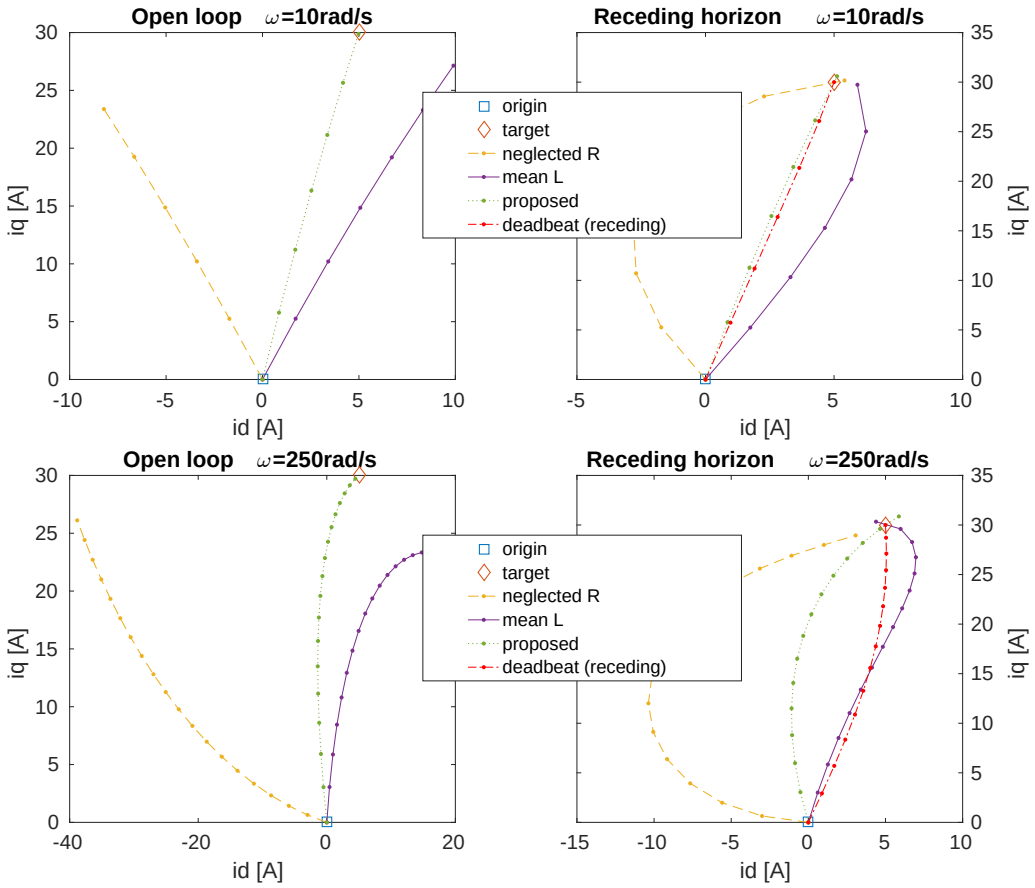

Figure 3. Comparison of studied versions of time-optimal control and deadbeat control on current reference step change from zero to $[5, 30]$A for modified parameters of the system with lower inductance at $\omega = 10$ rad/s (**top** row), and $\omega = 250$ rad/s (**bottom** row). The difference of the solutions in the origin is visible in open-loop strategy (**left**), its impact on the receding horizon reevaluation in each sampling period (**right**), sampling times are denoted by dots on the full lines.

In this case, simplifications of the time-optimal trajectory differ from the proposed solution. This is most obvious on the open-loop results, where only the proposed solution reaches the requested value, but the strategy with neglected resistance goes far to the left (negative i_d) and the one with averaged inductances far to the right (positive i_d). This tendency is corrected in the closed-loop due to recalculations of the trajectory in each time step. However, even with a correctly reached target, the strategy with neglected resistance generates a trajectory with very low i_d currents, and consequently reaches the setpoint in the longest time ($15\Delta t$). The strategy with averaged inductances takes a path with positive i_d currents and reaches the setpoint in $15\Delta t$. The proposed strategy is at low speed almost equivalent to the deadbeat controller, and reaches the setpoint in $14\Delta t$ equally with the deadbeat.

An important conclusion is that even for these parameters, the open-loop trajectory of the proposed control reaches the target setpoint. This implies that the approximation proposed in (21) is sufficiently accurate, in contrast to the simplified solutions.

4.3. Discussion of Results

The results of the controllers significantly differ for different parameters. When the stator resistance is low, it can be neglected in the time-optimal controllers, and the resulting controller yields in high speeds significantly faster transients than the deadbeat controller. However, when the effect of the resistance is higher, the TOC with neglected resistance provides a poor solution that is actually slower than the deadbeat solution and yields higher Joule losses. In such a case, the proposed TOC with resistance yields a better solution. The

only computationally slow operation is the sinh function, which needs to be computed for $\omega < \delta$. If computational cost is a concern, it is safe to use the deadbeat controller in this operating regime and switch to TOC only for higher speeds.

5. Experimental Results for IPMSM

A laboratory prototype of the IPMSM drive with the same parameters as in the simulation (28) was used to verify the approach experimentally. The test rig is displayed in Figure 4.

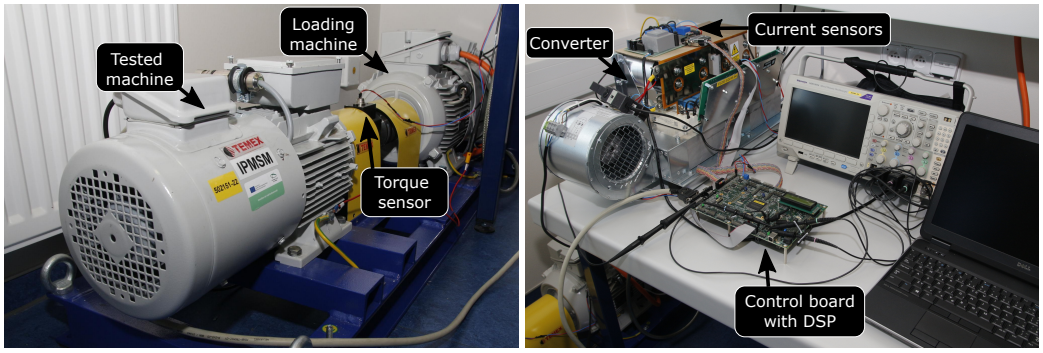

Figure 4. Photo of the test rig with the controlled IPMSM and loading induction machine (**left**), and the controlled converter, current sensors and the control board (**right**).

The rated power of the IPMSM drive is 4.5 kW, rated voltage 400 V, rated current 12.47 A rms, and rated speed 1500 rpm. The IPMSM drive is equipped with 12 bit absolute angular position encoder LARM ARC 405, torque sensor Burster 8661, voltage transducer LEM LV 25-P for converter dc-link voltage measurement, and current transducers LA 55-P for measurement of the stator phase currents. The switching frequency of the voltage-source converter supplying IPMSM is 10 kHz.

The current control strategies will be used to follow setpoint designed by optimal steady-state solution that respects stator resistance and different inductances as described in [4]. The full block diagram is displayed in Figure 5.

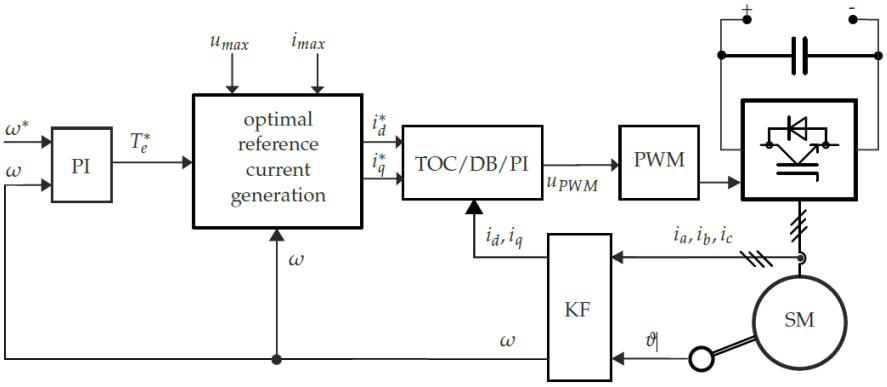

Figure 5. Block diagram of the tested closed loop controller.

This follows the conventional cascade structure, where the speed of the drive is controlled by a PI controller (or any other controller) yielding the requested torque, T_e^*. The requested stator current vector in the dq reference frame with elements i_d^* and i_q^* is calculated from the requested torque by an optimization scheme that minimizes Joule losses in the steady-state [4]. Specifically, the optimal setpoint is calculated as the intersection of the torque curve with the MTPA curve or with the field weakening (FW) curve. The method presented in [4] extends previous approaches (e.g., [2]) by explicit consideration of stator resistance. The effect of the stator resistance on the FW curve is visualized in Figure 6.

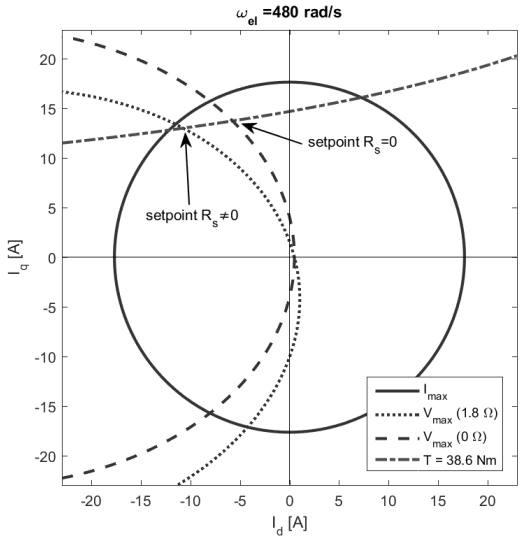

Figure 6. Visualization of optimal setpoints for rotor speed $\omega = 400$ rad/s. The optimal setpoint lies on the intersection of the FW curve with the iso-torque curve (T = 38.6 Nm). FW curve with correct resistance ($R_s = 1.8\ \Omega$) is compared to curve with neglected resistance ($R_s = 0\ \Omega$).

Note that the FW curve that does not consider that the resistance is symmetric around the x-axis, while the curve that considers that it is not. This means that the i_d current in the real drive has to be lower than predicted using the simplified FW curve. This mismatch has been achieved by using "safety" coefficient ζ, [2], $\overline{U} = \zeta U_{dc}/2$ where U_{dc} is the dc-link voltage. In real experiments, the safety coefficient for the simplified approach has to be set to $\zeta = 0.7$ to achieve good performance. The improved solution of [4] allows us to use higher safety coefficient, $\zeta = 0.9$ was found to be sufficient in our case. This improvement is achieved at a higher computational cost due to the need to solve roots of fourth-order polynomials.

In the experiments, the current control loop is either the proposed time-optimal controller (TOC), the standard truncated deadbeat controller (DB) from (27), or the FOC using the conventional PI controllers

$$u^*_{d,t} = k_p e_{d,t} + k_i \sum_{i=1} e_{t-i}, \quad e_{d,t} = (i_{d,t} - i^*_{d,t}),$$

and analogously for the q axis. Both the TOC and the deadbeat controllers are tuning free, but the performance of the PI controller depends on the choice of coefficients k_p and k_i (tuning). We have tuned the PI controller to yield the best overall performance. It is possible to re-tune the controller to obtain better results at one operating point, however, at the cost of deteriorating performance at another. However, the behavior of the control remains very similar for different tuning due to the fact that it is a pure feedback controller. The computational times of the control loop building-blocks are given in Table 1.

Table 1. Computational times of the control algorithm on DSP TMS320F28377S.

Computational Time	µs
data acquisition + KF	6.8
setpoint optimization	41.2
delay compensation + DB	1.5
TOC coefficient evaluation	1.5
TOC bisection for sin/sinh	18/28
modulation signals	5.8
total	74.8/84.8

The execution time of the TOC depends on the rotor speed. For lower speeds, the base functions are the hyperbolic functions (sinh,cosh), which are more expensive, while for higher speeds, the base functions are the sin and cos functions, which are cheaper.

Since the TOC controller is based on the assumption of the perfect state knowledge, we use the Kalman filter (block KF in Figure 5) to reconstruct the speed, position, and stator currents from the position and current measurements.

The performance of the controller is tested on a testing profile displayed in Figure 7.

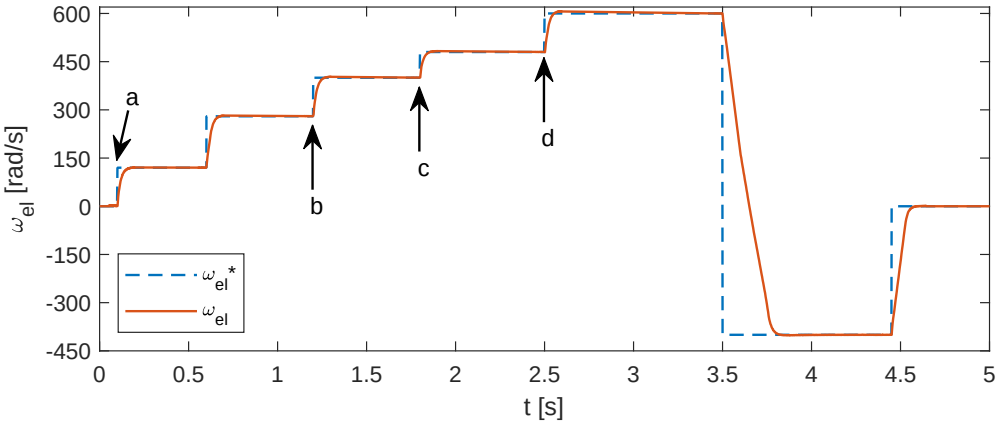

Figure 7. Speed profile of the experimental evaluation. Speed request is displayed in a dashed blue line, the actual speed in a red full line. Letters a, b, c and d indicate moments that are analyzed in detail in Figure 8.

Which is composed of multiple step changes of the requested rotor speed. Since the step change is high, the PI controller of the speed generates a request for the maximum possible torque. The optimization routine provides current setpoints corresponding to the best option at the given operating point. For low-speed operations, it selects points on the maximum torque per ampere curve. In the field weakening regime, it computes optimal currents for field weakening. References on the torque and currents remain almost constant for many sampling periods since the time-constant of the speed is much longer than that of the currents. To visualize the differences between the proposed controllers, we provide details of the current transient at the time of the step change at multiple operating points. These points are at different speeds $\omega = 0, 280, 400, 480$ for acceleration request and $\omega = 600$ rad/s for speed reversal request, see Figure 7 for illustration.

The resulting torque and current trajectories at selected operating points are displayed in Figure 8 in two modes: (i) time trajectories visualize the temporal convergence of the trajectories to setpoints displayed by dashed lines in the right subplots, and (ii) current *d*-*q* plane trajectories to the setpoints displayed by crosses in the left subplots. Note that at zero speed, the current trajectories of all controllers are very similar and equally fast. This is understandable since the TOC trajectory is almost a straight line at very low speeds. It starts deviating from a straight line with a higher speed, as can be noted for case (b) in Figure 8.

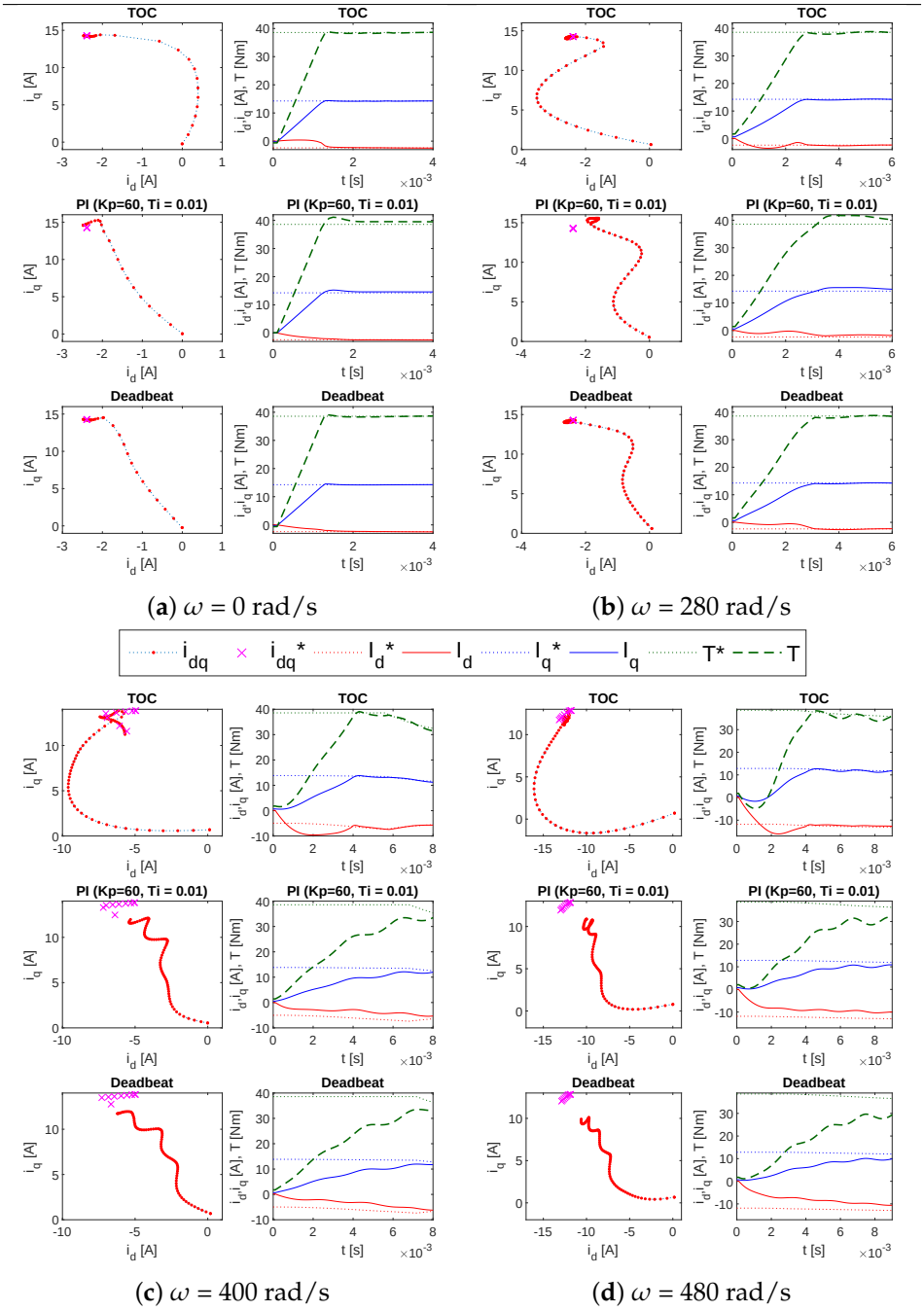

Figure 8. Details of torque and current trajectories at selected moments—(**a**–**d**)—of the experimental testing profile. For each transient, we plot the resulting trajectories for TOC controller (**top** row), PI controller (**middle** row), and deadbeat controller (**bottom** row). Trajectories of the currents in the *d*-*q* coordinates are displayed in the left subfigures with the requested current values denoted by crosses. Trajectories in the time domain are displayed in the right subfigures. The requested values of the torque and current are marked by dashed lines.

At $\omega = 280$ rad/s, the field weakening limit crosses the MTPA line, and the reference of the *d* current moves to negative values. At this moment, the TOC controller is able to reach the requested torque in 2.5 ms and remain stable at this value. The PI controller reaches the requested torque around the same time, but only due to the fact that it reaches the torque curve at different current values than requested. In an attempt to reach the requested currents, the torque request overshot, and it takes a while to settle it. The DB controller reaches the requested torque later, around 3 ms, but it is also able to remain stable

at this value. Even more obvious is the difference at $\omega = 400$ rad/s and $\omega = 480$ rad/s, where the TOC controller is able to reach the requested torque in 4 ms, contrary to the other controllers, that are not able to reach it in twice that time. Note that the TOC controller starts the transient with decreasing i_d current at the cost of decreasing the i_q current. This strategy yields a decrease of the torque for a very short time. However, this short time decrease allows a much faster increase of the torque in the second part of the transient. This demonstrates the ability of the TOC controller to optimize on a very long horizon. Performance of all controllers at the speed reversal moment at $\omega = 600$ rad/s is again comparable.

A summary of the settling times for all transients is provided in Table 2. The settling time was measured as the time after which the measured current is within 5% of the requested value.

Table 2. Comparison of settling time of different controllers for the transients in Figure 8. All times are given in milliseconds.

	i_d			i_q		
Step at Speed	**TOC**	**PI**	**DB**	**TOC**	**PI**	**DB**
$\omega = 0$ rad/s	1.8	1.8	1.8	1.3	4.7	1.3
$\omega = 280$ rad/s	2.8	10.0	3.1	2.7	9.5	3.0
$\omega = 400$ rad/s	4.5	11.2	8.1	4.1	17.6	8.6
$\omega = 480$ rad/s	4.0	22.5	16.0	4.3	18.6	17.5

As expected, the TOC has the most visible benefits at high speeds. While minimization of the speed of the transient is its primary objective, we would like to point out that the current trajectories of the TOC controller also exhibit lower oscillations. This is propagated into the torque trajectory, which is followed by TOC with lower oscillations than those provided by the PI and deadbeat controllers.

6. Conclusions

We have proposed a time-optimal control strategy for current control of the general synchronous motor drive, that considers also stator resistance and differences in stator inductances in the direct and quadrature axis. We have shown that the base functions of the optimal trajectory differ from those of the previous simplified solutions. We have derived a bisection-based optimization algorithm for the evaluation of the more accurate control strategy, which has only a minor increase in computational demands compared to previous simplified solutions.

The proposed strategy was able to reach the requested current in the minimum possible time. The difference to conventional PI or DB controllers is negligible at lower speeds; however, it provides significantly faster transients at higher speeds. On the testing prototype, TOC achieved a four times faster settling time than the PI and DB controllers at rotor speed of 480 rad/s. This is caused by the fact that TOC is a feed-forward controller increasing the tracking error at the beginning of the transient, which is not natural for a feedback controller.

While the controller is designed to minimize the time of the transient, we have found that it also provides more stable tracking of the required torque. The use of this control may thus benefit applications that require fast and accurate torque tracking such as high dynamic servo drives for robotics or manipulators.

Note that the proposed feed-forward strategy can be combined with any feed-back strategy, even with the conventional PI cascade. We believe that the proposed controller can be used as a universal building block complementing existing solutions. Exploring all potential benefits of the approach in combinations with different feedback solutions and different observers is left for future study.

Author Contributions: Methodology, V.Š. and L.A.; software, L.A. and A.G.; validation, A.G.; data curation, A.G.; writing—original draft preparation, V.Š., L.A. and A.G.; writing—review and editing, Z.P. and L.A. All authors have read and agreed to the published version of the manuscript.

Funding: This research was funded by the Ministry of Education, Youth and Sports of the Czech Republic under the project OP VVV Electrical Engineering Technologies with High-Level of Embedded Intelligence, CZ.02.1.01/0.0/0.0/18 069/0009855, project OP VVV Research Center for Informatics, CZ.02.1.01/0.0/0.0/16 019/0000765, and by UWB Student Grant Project no. SGS-2021-021.

Institutional Review Board Statement: Not applicable.

Informed Consent Statement: Not applicable.

Data Availability Statement: Data sharing not applicable.

Conflicts of Interest: The authors declare no conflict of interest. The funders had no role in the design of the study; in the collection, analyses, or interpretation of data; in the writing of the manuscript, or in the decision to publish the results.

References

1. Vas, P. *Vector Control of AC Machines*; Oxford University Press: Oxford, UK, 1990; Volume 22.
2. Preindl, M.; Bolognani, S. Optimal State Reference Computation With Constrained MTPA Criterion for PM Motor Drives. *IEEE Trans. Power Electron.* **2015**, *30*, 4524–4535. [CrossRef]
3. Preindl, M.; Bolognani, S. Model Predictive Direct Torque Control With Finite Control Set for PMSM Drive Systems, Part 1: Maximum Torque Per Ampere Operation. *IEEE Trans. Ind. Inform.* **2013**, *9*, 1912–1921. [CrossRef]
4. Eldeeb, H.; Hackl, C.M.; Horlbeck, L.; Kullick, J. A unified theory for optimal feedforward torque control of anisotropic synchronous machines. *Int. J. Control* **2017**, 1–30. [CrossRef]
5. Glac, A.; Šmídl, V.; Peroutka, Z.; Hackl, C.M. Dependence of IPMSM Motor Efficiency on Parameter Estimates. *Sustainability* **2021**, *13*, 9299. [CrossRef]
6. Jung, J.W.; Leu, V.Q.; Do, T.D.; Kim, E.K.; Choi, H.H. Adaptive PID speed control design for permanent magnet synchronous motor drives. *IEEE Trans. Power Electron.* **2014**, *30*, 900–908. [CrossRef]
7. Sira-Ramírez, H.; Linares-Flores, J.; García-Rodríguez, C.; Contreras-Ordaz, M.A. On the control of the permanent magnet synchronous motor: An active disturbance rejection control approach. *IEEE Trans. Control. Syst. Technol.* **2014**, *22*, 2056–2063. [CrossRef]
8. Humaidi, A.J.; Hameed, A.H. PMLSM position control based on continuous projection adaptive sliding mode controller. *Syst. Sci. Control Eng.* **2018**, *6*, 242–252. [CrossRef]
9. Rodriguez, J.; Kazmierkowski, M.; Espinoza, J.; Zanchetta, P.; Abu-Rub, H.; Young, H.; Rojas, C. State of the Art of Finite Control Set Model Predictive Control in Power Electronics. *IEEE Trans. Ind. Inform.* **2013**, *9*, 1003–1016. [CrossRef]
10. Preindl, M.; Bolognani, S. Model predictive direct torque control with finite control set for pmsm drive systems, Part 2: Field weakening operation. *IEEE Trans. Ind. Inform.* **2013**, *9*, 648–657. [CrossRef]
11. Preindl, M.; Bolognani, S. Model predictive direct speed control with finite control set of PMSM drive systems. *IEEE Trans. Power Electron.* **2013**, *28*, 1007–1015. [CrossRef]
12. Mariethoz, S.; Domahidi, A.; Morari, M. High-bandwidth explicit model predictive control of electrical drives. *IEEE Trans. Ind. Appl.* **2012**, *48*, 1980–1992. [CrossRef]
13. Gao, S.; Wei, Y.; Zhang, D.; Qi, H.; Wei, Y. A Modified Model Predictive Torque Control with Parameters Robustness Improvement for PMSM of Electric Vehicles. *Actuators* **2021**, *10*, 132. [CrossRef]
14. Fehér, M.; Straka, O.; Šmídl, V. Model predictive control of electric drive system with L1-norm. *Eur. J. Control* **2020**, *56*, 242–253. [CrossRef]
15. Li, L.; Zhou, W.; Bi, X.; Sun, X.; Shi, X. Second-Order Model-Based Predictive Control of Dual Three-Phase PMSM Based on Current Loop Operation Optimization. *Actuators* **2022**, *11*, 251. [CrossRef]
16. Šmídl, V.; Mácha, V.; Janouš, Š.; Peroutka, Z. Analysis of cost functions and setpoints for predictive speed control of PMSM drives. In Proceedings of the 2016 18th European Conference on Power Electronics and Applications (EPE'16 ECCE Europe), Karlsruhe, Germany, 5–9 September 2016; pp. 1–8.
17. Besselmann, T.; Lofberg, J.; Morari, M. Explicit MPC for LPV Systems: Stability and Optimality. *IEEE Trans. Autom. Control* **2012**, *57*, 2322–2332. [CrossRef]
18. Clarke, F.H. *Functional Analysis, Calculus of Variations and Optimal Control*; Springer: Berlin/Heidelberg, Germany, 2013.
19. He, F.; Huang, Q. Time-Optimal Trajectory Planning of 6-DOF Manipulator Based on Fuzzy Control. *Actuators* **2022**, *11*, 332. [CrossRef]
20. Bianchi, N.; Bolognani, S.; Zigliotto, M. Time optimal current control for PMSM drives. In Proceedings of the IEEE 2002 28th Annual Conference of the Industrial Electronics Society, IECON 02, Seville, Spain, 5–8 November 2002; Volume 1, pp. 745–750.

21. Konghirun, M.; Xu, L. A fast transient-current control strategy in sensorless vector-controlled permanent magnet synchronous motor. *IEEE Trans. Power Electron.* **2006**, *21*, 1508–1512. [CrossRef]
22. Li, S.; Xu, L. Minimum-time flux-linkage transition for PMSM control with minimum number of inverter switching. In Proceedings of the ICEMS'2001, Fifth International Conference on Electrical Machines and Systems (IEEE Cat. No.01EX501), Shenyang, China, 18–20 August 2001; Volume 2, pp. 1207–1210.
23. Xu, L.; Li, S. A fast response torque control for interior permanent-magnet synchronous motors in extended flux-weakening operation regime. In Proceedings of the IEMDC 2001, IEEE International Electric Machines and Drives Conference (Cat. No.01EX485), Cambridge, MA, USA, 17–20 June 2001; pp. 33–36.
24. Lee, J.S.; Lorenz, R.D.; Valenzuela, M.A. Time-optimal and loss-minimizing deadbeat-direct torque and flux control for interior permanent-magnet synchronous machines. *IEEE Trans. Ind. Appl.* **2014**, *50*, 1880–1890. [CrossRef]
25. Šmídl, V.; Janouš, Š.; Peroutka, Z.; Adam, L. Time-optimal current trajectory for predictive speed control of PMSM drive. In Proceedings of the 2017 IEEE International Symposium on Predictive Control of Electrical Drives and Power Electronics (PRECEDE), Pilsen, Czech Republic, 4–6 September 2017; pp. 83–88.
26. Zhang, Z.; Jing, L.; Wu, X.; Xu, W.; Liu, J.; Lyu, G.; Fan, Z. A deadbeat PI controller with modified feedforward for PMSM under low carrier ratio. *IEEE Access* **2021**, *9*, 63463–63474. [CrossRef]
27. Schraudolph, N.N. A fast, compact approximation of the exponential function. *Neural Comput.* **1999**, *11*, 853–862. [CrossRef] [PubMed]

Disclaimer/Publisher's Note: The statements, opinions and data contained in all publications are solely those of the individual author(s) and contributor(s) and not of MDPI and/or the editor(s). MDPI and/or the editor(s) disclaim responsibility for any injury to people or property resulting from any ideas, methods, instructions or products referred to in the content.